Journal of Simulation and Analysis of Novel Technologies in Mechanical Engineering
15 (4) (2023) 0005~0015

Research article

Numerical solution of hovering propeller performance at various blade pitch angles and revolutions with different turbulence models

Behrooz Shahriari[1*], Mohammad Reza Hashemi[2]

[1]*Faculty of Mechanics, Malek Ashtar University of Technology, Isfahan, Iran.*
[2]*PhD student, Mechanical Engineering, University of Birjand, Birjand, Iran.*

[*]shahriari@mut-es.ac.ir

(Manuscript Received --- 07 Sep. 2023; Revised --- 20 Oct. 2023; Accepted --- 25 Oct. 2023)

Abstract

In this research the validation of different turbulence models of a hovering propeller at different pitch angles and revolutions has been investigated. For this purpose, the pressure on the propeller surface at different cross sections has been calculated numerically by six different turbulence models and compared with the experimental data. In the first part, the effects of changing the blade angle have been discussed, in this case, the angles of 0, 2, and 12 degrees have been selected. The results showed that changes in the pitch angle of the propeller have led to an increase in the error rate of numerical calculations. At a high pitch angle and in the same chord section, the highest amount of error is produced in leading edge section of the propeller, among which the best model in terms of production error is the k-e RNG. Also, due to the possibility of the formation of shock waves, the S-A and k-e standard models have very large errors, which shows these models' inability to simulate rotating flow with shock waves.

Keywords: Propeller, Blade pitch angle, Turbulence model, Hover, Shock wave.

1- Introduction

One of the most important parts of any moving vehicle is its propulsion system. In all types of aircraft and submarines, the task of the propulsion system is to produce thrust force to overcome the drag force. Therefore, researchers are looking for increasing efficiency and reducing costs in this part, which will increase the total efficiency [1]. In helicopters, in addition to overcoming the drag force, the propulsion system must also compensate for the weight of the helicopter by producing lift force [2]. Due to the geometry of the propeller as well as the nature of the rotating flow created by it, the aerodynamic analysis of the propeller is a complex matter [3]. One of the basic problems in solving the flow field of rotating objects such as propellers is to choose the correct solution method so that a proper estimate of the flow field and then the forces can be obtained. In the study of the flow around the propeller, it is possible to use the method of solving the potential (inviscid) flow as well as the viscous flow in the numerical solution, especially the RANS method. In the method of solving the potential flow, which included a wide range of problems related to the propeller, there was a need for basic information such as

determining the initial location of the trailing edge vortex, which increased the complexity of this method [4]. With the expansion of numerical solution codes, especially RANS, and to increase the accuracy and ensure the correctness of the results, it was proposed to solve the viscous flow around the propeller [5]. One of the major problems in solving CFD is choosing the appropriate turbulence model, boundary layer, and grid type to correctly predict flow separation [6]. Kuiper [7] showed that to analyze the submarine propeller, CFD and experimental data must be used to overcome the shortcomings of the potential method (viscosity term). One of the most fundamental problems of using the potential method is the lack of analysis of the propeller in stall conditions as well as in the transonic regime [8]. According to Wake's research [9], the use of unstable Navier-Stokes equations has more advantages than Euler and non-viscous equations, but its main problem is the increase in cost and solution time. For example, solving the viscous term in Navier-Stokes equations has led to a 25% increase in calculation time, especially at high Reynolds numbers. However, the use of the mentioned method had a very good match with the experimental data for the hovering helicopter. Andronikos et al. [10] in the validation of the numerical analysis of the propeller in the ground effect concluded that the potential model did not have a good prediction of the flow pattern on the earth's surface at very close distances between the propeller and the ground. The reason was the ground is located in the downwash of the propeller and creates separation on it so that the potential method is not capable of modeling this state. By increasing the distance between the propeller and the ground, the potential method results had a better match with the experimental data. Alom [11] [12] and Kamoji [13] showed that increasing the Reynolds number causes the separation to be delayed on the rotor sections and as a result, the power coefficient increases. Bennaya et al.[14] showed that, to validate the thrust and pressure coefficients of the submarine propeller, the most appropriate turbulence model is k-e RNG and the highest error is related to the k-w model. With the increase of the propeller advance ratio, the amount of errors increased, but still, the biggest difference between the CFD and experimental data was related to the k-w model. Finally, they concluded that the use of the CFD method in simulating the flow field around the hydrodynamic propeller is very efficient and reliable. Sezen et al. [15] showed that the increase in blade loading leads to an increase in instability in the vortices produced by the propeller, which completely changes the characteristics of the propeller's slipstream. By moving downstream, the instabilities of flow have increased, which is the reason for the breaking of eddies. They showed that the k-w turbulence model, compared to other models, could not predict very well the location of the vortex breakdown. Wang et al. [16] showed that under heavy loading conditions, The elliptic instability on each helicoidal tip vortex evolves into two interlaced spiral vortex branches. As tip vortices continue to evolve downstream, the vortex branches begin to interact with the branch structures of adjacent tip vortices, leading to the breakdown of the tip vortex system. Comparisons of DES and LES models demonstrated that LES can resolve more turbulence details at the same time and grid resolution than its counterpart but predicts early tip vortex structure breakdown, thus losing the near-field

coherence observed in the IDDES results. Pawar et al. [17] investigated the difference between sliding mesh and MRF methods in simulating the flow around a subsurface propeller. Their results indicated that the two mentioned methods did not differ much from each other and only when using the sliding mesh, the vortices formed in the trailing edge were slightly smaller in dimension. Loureiro et al. [18] showed that in advanced ratio velocities and low Reynolds numbers, the use of the Blade element momentum theory method, in addition to being very economical, also provides acceptable results for small propellers. With the increase of advanced ratio, the matching results are not suitable and the use of the CFD method is suggested. Jiang et al. [19] showed that using the RANS method can well capture the main flow field features and predict the mean propeller loads. DES model also shows more details than RANS models and also predicts the propeller loads with much higher fluctuations than RANS. In addition, it is found that the phase-averaged evolution course of the propeller force predicted by the DES model is almost the same as that directly predicted by the RANS model. According to Tu's research [20], the results of solving the flow around propeller hydrodynamics are highly dependent on mesh density, mesh type, and turbulence model. The hexahedral grid has provided better results than the polyhedral grid in all advanced ratios.

According to the previous works, choosing the best turbulence model as well as the type of mesh around the propeller is an important issue in the CFD analysis of the flow around it. One of the important aspects of the current research is to investigate the pressure coefficient error of 6 commonly used turbulence models with experimental data. For this purpose, the pressure coefficient in different chord sections and cross-sections of the propeller at different blade pitch angles and revolutions have been investigated so that a good view of the exact location of the maximum error of the turbulence models can be obtained. This work ultimately reduces the amount of total error presented in the thrust and torque coefficients in different advanced ratios and provides a suitable reference for choosing the best turbulence model with the highest efficiency and the lowest number of meshes for all types of helicopter blades and airplane propellers.

2- Turbulent model

To predict the turbulent flow, the turbulence model is used to solve the Navier-Stokes equation. Due to the nature and characteristics of turbulent flow, all variables related to it such as pressure, speed, temperature, etc. are variables based on time and place. One of the best methods for simulating instantaneous turbulence flow is to use the DNS model in solving the Navier-Stokes equation. Yang and Griffin [21] showed that using the DNS method in solving complex turbulent flows with high Reynolds numbers is very time-consuming and expensive. Calculation time estimation in this method is based on grid points, which naturally required a very high number of grids to solve complex turbulent flows. Therefore, the use of averaged Navier-Stokes equations regarding the propeller flow is much more economical and is a suitable choice. In this method, instantaneous values are equal to the sum of mean and fluctuating parts ($u_i = \bar{u} + u'$).

2-1 k-ε turbulence model and its variants

k-ε can be considered the most famous and widely used turbulence model in solving a

wide range of problems, which includes several subgroups. In this model, there are two transfer equations to calculate turbulent stresses on eddy viscosity, which include turbulence kinetic energy and dissipation rate [22]. Model parameters are calibrated by using data from a number of benchmark experiments such as pipe flow, flat plate, etc. k-ε Contains submodels for compressibility, buoyancy, combustion, etc. In addition to all the advantages of this model, it has not provided a proper prediction in some flow fields. For example, Balabel and Askary [23] showed that in three types of jet flow (free round jet, the impinging jet problem, and the wall jet problem) that the linear turbulence models are found to give better predictions than the nonlinear models in simple jet flow (non-impinging). Shin et al. [24] extracted the value of the dissipation rate using mean-square vorticity fluctuation. Their results showed that this model has a much better prediction of the spreading rate of both planar and round jets. Also, this method provided an acceptable solution in flows with a strong adverse pressure gradient, swirling flow, and separations than the conventional model. Yakhot and Orszag [25] represented a newer model of k-e called k-e (RNG). In this model, Constants in the k–ε equations are derived analytically using renormalization group theory, instead of empirically from benchmark experimental data, and the Dissipation rate equation is modified. This method is suitable for complex shear flows and flows with high-strain rates, swirl and separation.

2-2 k-ω turbulence model and its variants

The second most used model in engineering problems is k-w. Similar to k-ε models, the Standard k-ω model solves a transport equation for turbulence kinetic energy (k) for determination of turbulent eddy viscosity [26]. In this method, the value of dissipation rate I has been replaced by turbulence frequency (w). The major difference between the k-w and k-e models is often in the vicinity of the solid boundary and the boundary condition of the wall. Adanta et al. [27] showed that despite the increase in calculation cost and time, it is better to use the k-w model instead of k-e to understand the physics of water wheel flow more correctly. The reason for this is Improved behavior under an adverse pressure gradient. Zhang et al. [28] showed that the k-w model is very sensitive to free-stream conditions and no difference between the k-w model and DES can be observed in the estimation of the drag force of the full-scale sedan vehicle. The improved k-w model was extracted by Menter [29] under the title k-ω SST (Shear Stress Transport).

The SST k–ω model uses a blending function to gradually transition from the standard k–ω model near the wall to a high-Reynolds-number version of the k– ε model in the outer portion of the boundary layer [30]. SST model generally gives accurate prediction of the onset and the size of separation under adverse pressure gradient. The k-ω SST model is available in many commercial CFD problems, and the popularity of the model increases for the solution of the hydrodynamic problems because of the several advantages in comparison to other models [31].

2-3 One equation turbulence models

Spalart and Allmaras (S-A) [32] presented a one-equation model, which, unlike the previous one-equation models, its results are local, which means the results at one point do not depend on other points. As a result, in this case, there is a compatibility

of grids with each structure and solver of the Navier Stokes equation, whether in two-dimensional or three-dimensional mode. One of the main advantages of this model compared to k-e is the simplicity in imposing the freestream and wall boundary conditions [33]. This model is mainly intended for aerodynamic and turbomachinery applications with mild separation such as supersonic and transonic flows over airfoils and boundary-layer flows [34]. Casseer and Ranasinghe [35] showed that among all the turbulence models in the numerical solution, the highest agreement between the CFD and experimental data in the case of a Ceiling Fan sample is related to the S-A model. Paciorri et al. [36] showed that using the S-A model in hypersonic flow, considering laminar separation and turbulent reattachment, there is a very good agreement with experimental data. A very important point regarding the work of Paciorri et al. is laminar separation. In fact, the main weakness of this model is in predicting the transition of the boundary layer and exposure to intense turbulence. Because of what was said, Medida and Baeder [37] stated that the use of the S-A model causes an overestimation in the airfoil lift and drag, especially in the region near the stall.

3- Numerical approach

3-1 Model and strategy

In order to perform the numerical simulation, Ansys software has been used. Fig. 1 shows the propeller used in the software and the coordinate system. The blade's span length is 2.286 m and its chord section is NACA 0012 airfoil. In the numerical solution, the governing equations are discretized based on the finite volume method. Temporal and spatial discretization was done by using a second-order scheme to increase the accuracy of the solution. A flow solver with a SIMPLE type solution algorithm was imposed on the calculations. Table 1 shows the turbulence models used in the research.

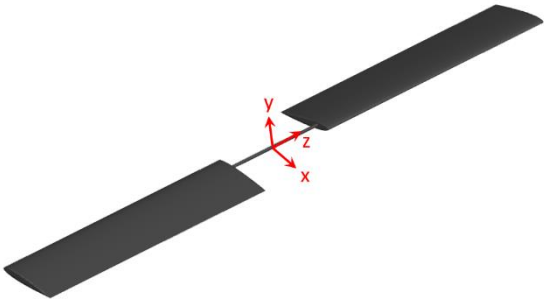

a) Propeller coordinate system

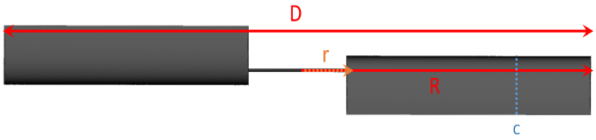

b) Propeller parameters

Fig. 1 The propeller used in numerical simulation

Table 1: Turbulence models used in the research

One equation model	Two equation mode
Spalart-Almaras (S-A)	k-e standard
	k-e RNG
	k-e realizable
	k-w standard
	k-w SST

Propeller rotational motion was modeled by using MRF (Multiple Reference Frame) techniques and during the simulations, the convergence of the propeller variables (i.e., pressure, velocity, etc.) was checked. In the numerical solution, a cylindrical computing domain around the propeller was used.

3-2 Boundary condition and grid independency

Fig. 2 shows the boundary conditions used in the numerical solution and the location of the propeller in the middle of the cylinder, where the distance from its tip to the top of the domain is equal to 5D (D is the propeller diameter), from the back is equal to 10D, and from the front is equal to 5D [38].

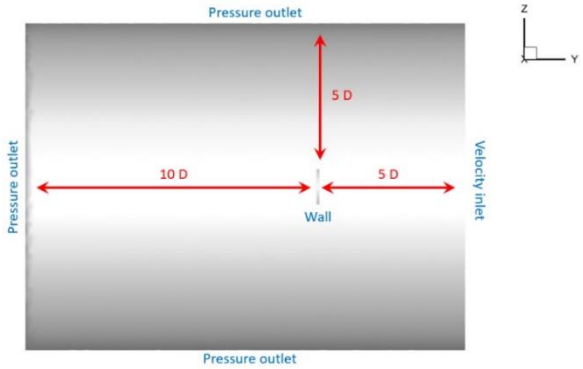

Fig. 2 Domain solution and the distance of the propeller to its boundaries.

The mesh used in this research is an unstructured type (Fig. 3) and at each stage of solving the value of y^+ was within the acceptable limit for each of the turbulence models.

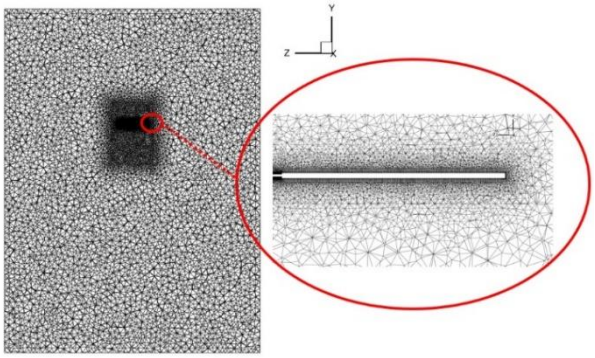

Fig. 3 A view of the mesh used in the numerical solution

Since the increase in the number of meshes leads to an increase in the calculation time and the resulting costs, therefore, the minimum number of meshes should be used. For this purpose, the grid independence carried out in the research is shown in Fig 4. As can be seen, after 6.4 million meshes, there is no noticeable change in the output of the solution, which is the thrust force. Therefore, the number of meshes has not exceeded 6.4 million in all solutions.

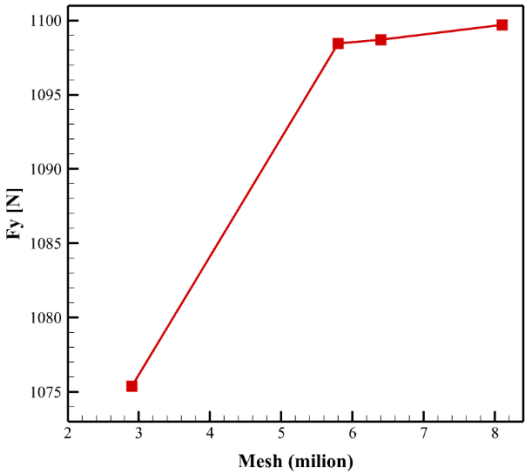

Fig. 4 Grid independence conducted in research.

4- Results

The results of the numerical solution are represented for three blade cross section that they are r/R=0.5, 0.68 and r/R=0.96. In order to observe the effects of changing blade angles and rotational speeds, the negative pressure coefficient on the upper surface and lower surface of the blade ($-Cp_u$ and $-Cp_l$) are calculated and compared with experimental data [39].

4-1 The effects of changing the pitch angle of the blade

In this part, the blade pitch angles were selected 0, 2, and 12 degrees and its rotational speed in all cases is 1500 rpm. Fig. 5 shows the comparison between different turbulent models with experimental data at different r/R for 0-degree pitch blade angle. As shown in Fig. 5a, in section r/R=0.5 the difference between the numerical solution and experimental data is very low but at X/C=0.12 the best models were k-w (SST and standard), k-e (RNG and realizable). By

approaching to trailing edge, the accuracy of all turbulent models was the same.

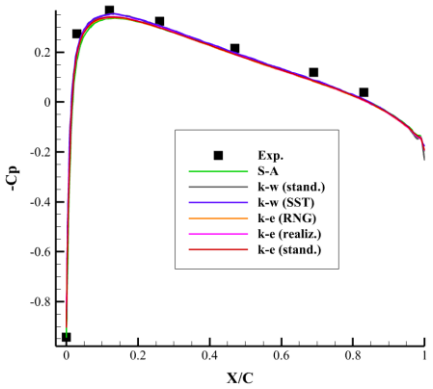

a) r/R=0.5

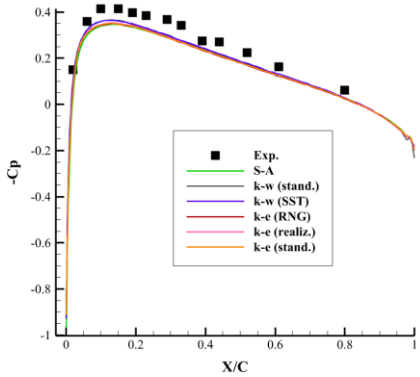

b) r/R=0.68

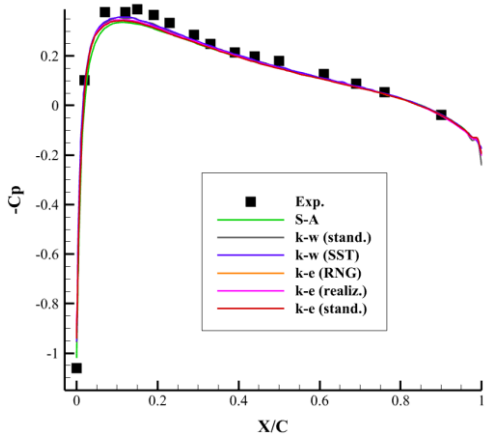

c) r/R=0.96

Fig. 5 Comparison between numerical and experimental data (pitch blade=0 and rpm=1500).

In section r/R=0.68 and X/C=0.15, the numerical solution and experimental data are in acceptable agreement. By moving downstream, the solution difference is increased. Fig. 6 shows the percentage of absolute error for each turbulent model at chord section X/C=0.19 and X/C=0.79. As can be seen in Figure 6, in the chord section of the leading edge, the error value of the models is much higher than that of the chord section near the trailing edge. The k-w SST model has the lowest error at the leading edge, which is equal to 12.4%, but near the trailing edge of the propeller, the k-e RNG model is the best with an error percentage of 0.12.

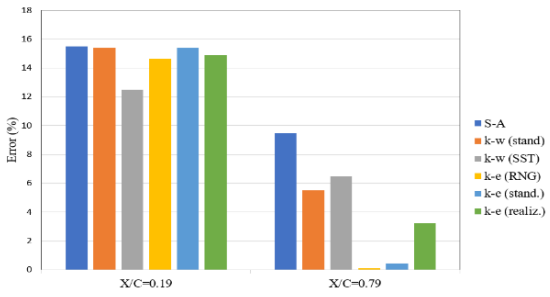

Fig. 6 Error bar for different turbulent model at X/C=0.15 and X/C=0.79 (pitch=0, rpm=1500, r/R=0.68).

By approaching the tip of the propeller, all the models have a good match with the

experimental data, but the weakness and deviation of S-A are observed in the part of the leading edge and the trailing edge (Fig. 5c). As the pitch angle of the propeller increases, the pressure coefficient has also changed. Fig. 7 shows the pressure coefficient on the propeller surface at a pitch angle of 2 degrees and a revolution of 1500 in different cross sections. In the section r/R=0.5 and the initial position of the measurement chord section (i.e. X/C=0), all the models had a good match with the experimental data. By moving towards the downstream sections, the solution difference is greater, and at X/C=0.12, the k-w models have the weakest performance, where the k-w standard error is equal to 5.8% and the k-w SST is equal to 5.1% (Fig. 8). At section X/C=0.26, the k-w SST error reached 7.14%, which was more than the previous section. The best model with a suitable prediction of the pressure coefficient was the k-e RNG model with an error percentage of 1.7. At the last chord section and near the tip of the propeller, the deviation of the data has already increased, and the worst model is k-w SST with an error of 33.3% and the best model is k-e RNG with an error of 14.1%. Fig. 9 shows the pressure coefficient on the propeller at a pitch angle of 12 degrees. As can be seen, there is a large difference between the selected turbulent models in high pitch blade angles. In all cross sections, the most critical location is at the leading edge, where the difference between the turbulence models and the difference between experimental and all CFD data is high. An important point is the inappropriate prediction of the S-A single equation model in all stages. By comparing Fig. 10 and 8, it can be seen that, at chord sections X/C=0.12 and X/C=0.26, there is no difference between the errors, and the difference is less than 5% for all models but the Ka-Epsilon model has a 6% increase in error, which Among them, it was the highest amount. The major solution error among all turbulence models occurred in the cross section near the trailing edge. Increasing the pitch angle of the propeller has led to an increase in the error rate in all models at this cross section. k-w SST, S-A, k-w standard, and k-e realizable models have the highest amount of error which are 49.52, 50.9, 48.57, and 47.14 respectively. As in the previous parts, the k-e RNG model has the least with a 38 percent error. According to Fig. 11, at the same chord section near the leading edge of the propeller, the amount of errors is reduced by moving toward the tip of the propeller.

4-2 The effects of changing the propeller revolution

In this section, the change in propeller revolution with a fixed pitch angle is investigated. For this purpose, the propeller is placed at a fixed pitch angle of 8 degrees and its revolution value is 650 and 2300. Fig. 12 shows the pressure coefficient on the propeller surface at a pitch angle of 8 degrees and a revolution of 650 degrees. According to Fig. 12a, between the chord section X/C=0.03 and X/C=0.12, the k-w SST turbulence model has a higher-pressure coefficient than the experimental test, which naturally indicates the measurement error of this model. But the k-e standard and S-A models have lower pressure coefficients than the experimental data, and the greater deviation is related to the k-e standard.

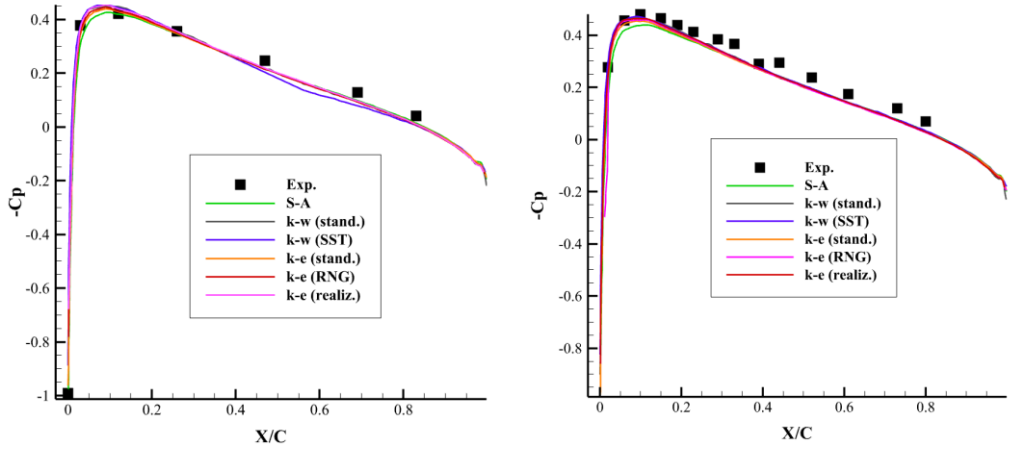

a) r/R=0.5 b) r/R=0.68

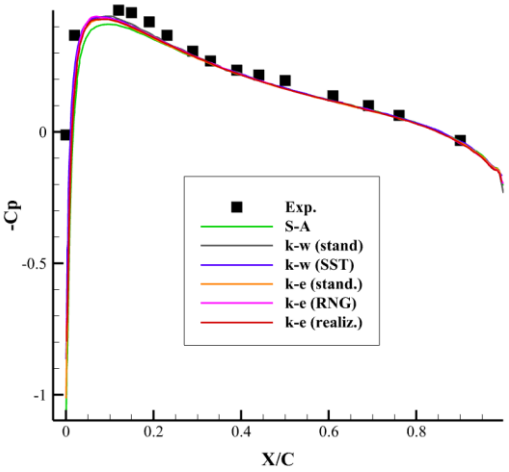

c) r/R=0.96

Fig. 7 Comparison between numerical and experimental data (pitch blade=2 and rpm=1500)

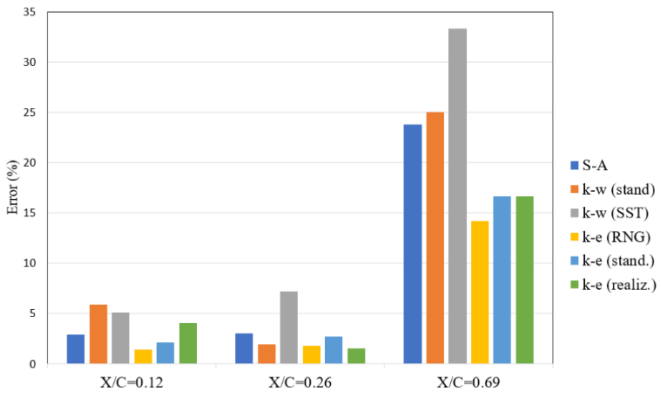

Fig. 8 Error bar for different turbulent model at X/C=0.12, X/C=0.26 and X/C=0.69 (pitch=2, rpm=1500, r/R=0.5)

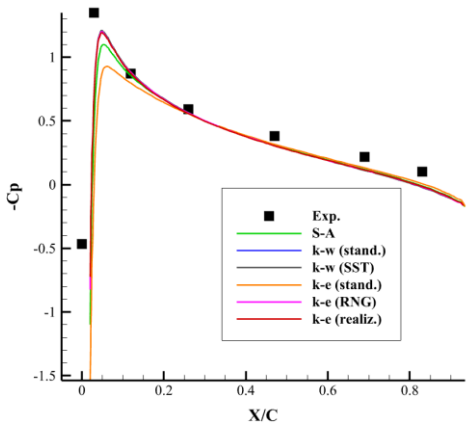

a) r/R=0.5

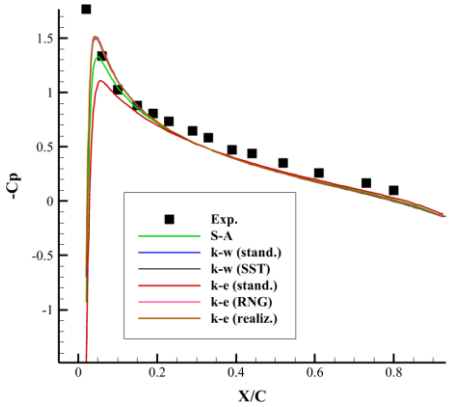

b) r/R=0.68

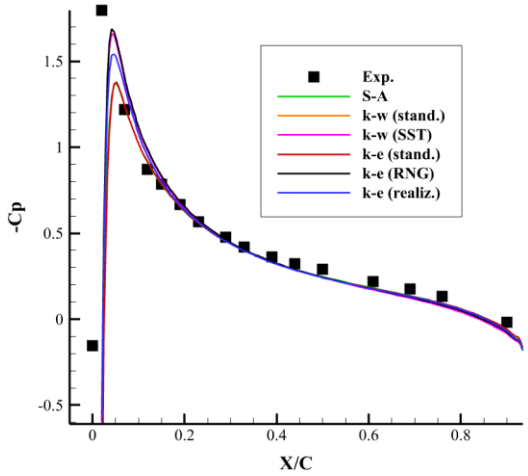

c) r/R=0.96

Fig. 9 Comparison between numerical and experimental data (pitch blade=12 and rpm=1500)

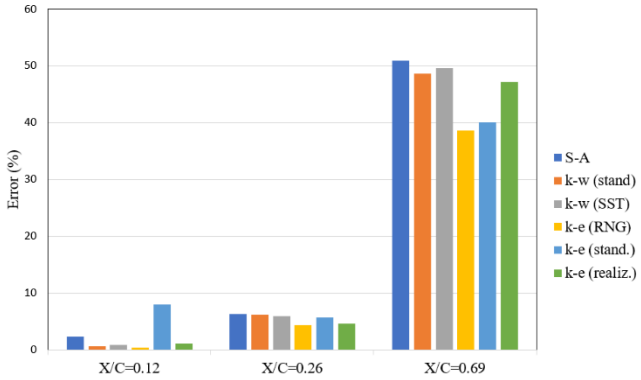

Fig. 10 Error bar for different turbulent model at X/C=0.12, X/C=0.26 and X/C=0.69 (pitch=12, rpm=1500, r/R=0.5)

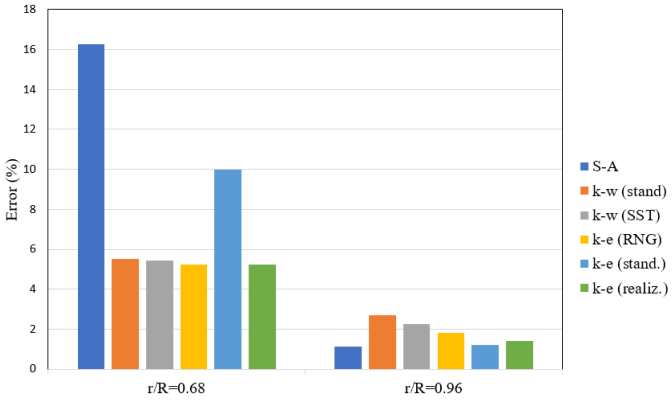

Fig. 11 Error bar for different turbulent model at X/C=0.19 (pitch=12, rpm=1500)

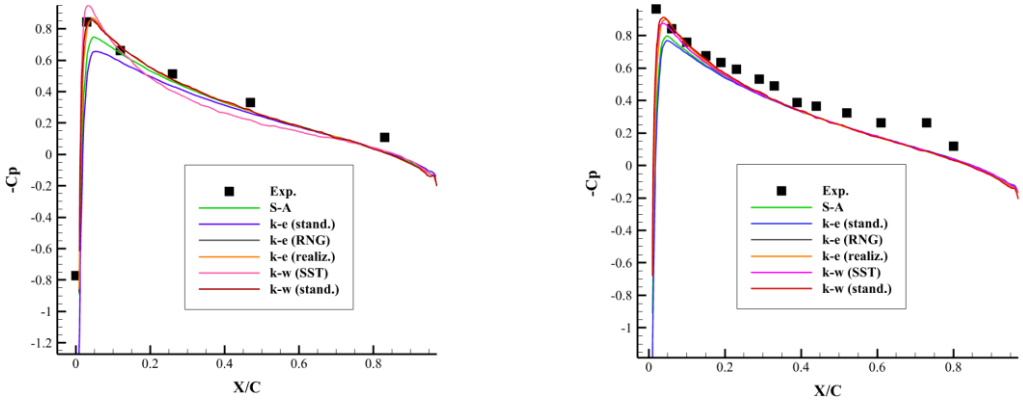

a) r/R=0.5 b) r/R=0.68

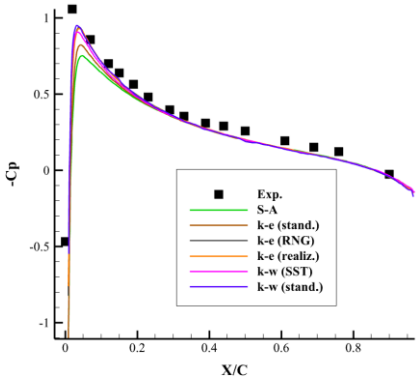

c) r/R=0.96

Fig. 12 Comparison between numerical and experimental data (pitch blade=8 and rpm=650)

As can be seen, the most matching is related to k-e RNG and k-w standard models. In the middle chord sections, the k-w SST model has a lower pressure coefficient than the experimental data, which has reduced the amount of deviation and solution error at the trailing edge. In the other two sections (Fig. 12 b and c), the k-w SST model has a better match than the previous section, but the standard S-A and k-e models have performed poorly in calculating the pressure coefficient. The increase in propeller speed in sections r/R=0.5 and r/R=0.68 is not much different from what was said in the previous section, but in this case, the k-w SST model showed less error than before. At the tip of the propeller and r/R=0.96, due to the increase in the

revolution of the propeller, there is a possibility of creating shock waves, which can be considered a critical location from this point of view. As shown in Fig. 13 c, after the chord section X/C=0.12, a sharp decrease in the pressure coefficient is observed. In this case, the S-A and k-e standard models had a very poor match with the experimental data and predicted the sudden pressure change far from reality. Fig. 14 shows the percentage of error in chord sections X/C=0.12 and X/C=0.39 (before and after sudden pressure change) at an 8 degrees pitch angle and 2300 revolutions. As can be seen, in X/C=0.12, the highest error is related to the S-A and k-e standard models with values of 26.57 and 18.89 percent. In this cross section, four other turbulence models have a good match with the experimental data, among which the error of the k-w SST and k-w standard models are equal to 0.51% and 0.17%, respectively, which have the best match. At section X/C=0.39, two k-w SST and k-w standard models still have an error of less than 1%, which shows the very appropriate prediction of these two models in rotating flows with sudden pressure changes in the chord section. Regarding the k-e RNG and k-e realizable models, the error value at the X/C=0.12 section is 2.51 and 0.77, respectively, and at the X/C=0.39 section, the error value is 2.48 and 6.38 percent.

5- Conclusion

In this research, to validate a hovering propeller, 6 popular and widely used RANS models have been investigated. In the first section of the study, the propeller is set at a fixed revolution of 1500 and its pitch is 0, 2, and 12 degrees. The results of this section showed that, at zero pitch angle and cross-section r/R=0.5, there is a good agreement between all turbulence models with experimental data. Approaching the tip of the propeller increases the amount of error, and at the cross-section r/R=0.68, the highest amount of error produce at the leading edge of the propeller. At the same cross-section, increasing the pitch angle of the propeller has led to an increase in the error rate of all turbulence models in the leading edge. In the second section of the study, the pitch angle is set to 8 degrees and the effects of the change in the revolution on the pressure coefficient are investigated. The results obtained from this section also showed that at 650 rpm, the highest error is related to the S-A and k-e standard models. With the increase in the propeller revolution and the possibility of the formation of shock waves, a sudden change of pressure has occurred in the section near the leading edge. Three turbulence models (k-e RNG, k-w SST, and k-w standard) had a very good ability to simulate this sudden pressure change. In general, it can be said that the k-e RNG turbulence model has a lower error percentage than other models in all cases, and at high propeller revolution, it can also simulate the pressure changes caused by shock waves. In terms of the number of meshes and solution time, this model has been more suitable in rotational flows with high revolution and pitch.

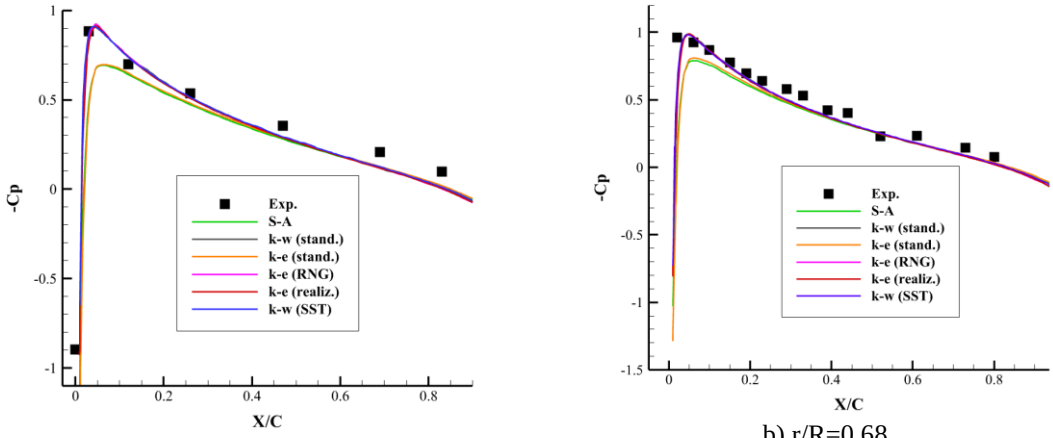

a) r/R=0.5

b) r/R=0.68

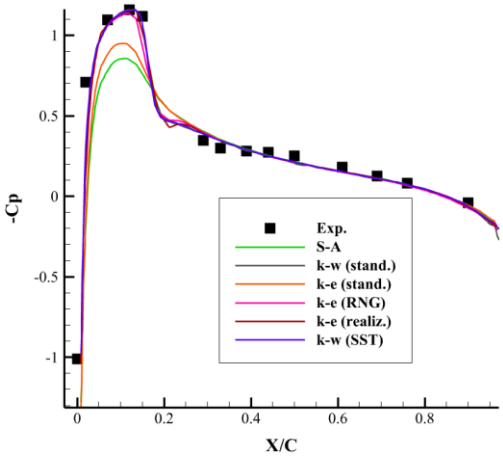

c) r/R=0.96

Fig. 13 Comparison between numerical and experimental data (pitch blade=8 and rpm=2300)

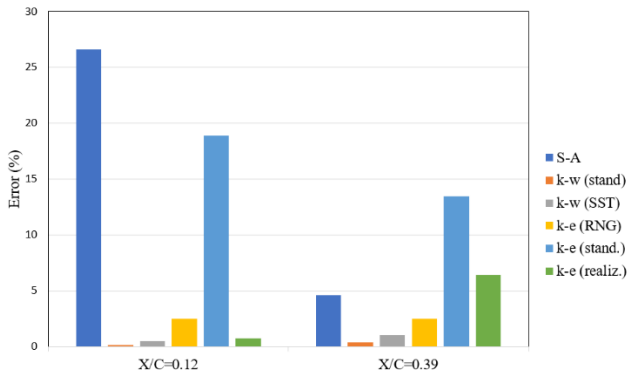

Fig. 14 Error bar for different turbulent model at X/C=0.12 and X/C=0.39 (pitch=8, rpm=2300, r/R=0.96)

References

[1] Eqbal, S., Fernando, N., Marino, M. and Wild, G. (2018). Hybrid propulsion systems for remotely piloted aircraft systems. *Aerospace*, 5(2), 34-52.

[2] Yeo, H. (2019). Design and aeromechanics investigation of compound helicopters. *Aerospace Science and Technology*, 88, 158-173.

[3] Huyer, S.A. and Snarski, S.R, (2003). Analysis of a turbulent propeller inflow. *Journal Fluids Eng.*, 125(3), 533-542.

[4] Rhee, S.H. and Joshi, S. (2003). January CFD validation for a marine propeller using an unstructured mesh based RANS method, *Fluids Engineering Division Summer Meeting*, 36, 1157-1163.

[5] Funeno, I. (2002). On viscous flow around marine propellers hub vortex scale effect, *J. Kanasai Soc. Japan*, (238), 17-27.

[6] Strawn, R.C., Caradonna, F.X. and Duque, E.P, (2006). 30 years of rotorcraft computational fluid dynamics research and development. *Journal of the American Helicopter Society*, 51(1), 5-21.

[7] Kuiper, G. (2010). New developments and propeller design. *Journal of Hydrodynamics, Ser. B*, 22(5), 7-16.

[8] Egolf, T.A. and Sparks, S.P. (1987). A Full Potential Rotor Analysis with Wake Influence Using an Inner-Outer Domain Technique. *Journal of the American Helicopter Society*, 32(3), 15-24.

[9] Wake, B.E. and Sankar, L.N. (1989). Solutions of the Navier-Stokes Equations for the Flow About a Rotor Blade. *Journal of the American Helicopter Society*, 34(2), 13-23.

[10] Andronikos, T., Papadakis, G., Riziotis, V.A., Prospathopoulos, J.M. and Voutsinas, S.G, (2021). Validation of a cost effective method for the rotor-obstacle interaction. *Aerospace Science and Technology*, 113, 1-13.

[11] Alom, N. and Saha, U.K, (2019). Influence of blade profiles on Savonius rotor performance: Numerical simulation and experimental validation. *Energy Conversion and Management*, 186, 267-277.

[12] Alom, N. and Saha, U.K, (2019). Evolution and progress in the development of savonius wind turbine rotor blade profiles and shapes. *Journal of Solar Energy Engineering*, 141(3).

[13] Kamoji, M.A., Kedare, S.B. and Prabhu, S.V (2009). Performance tests on helical Savonius rotors. *Renewable Energy*, 34(3), 521-529.

[14] Bennaya, M., Gong, J.F., Hegaze, M.M. and Zhang, W.P (2013). Numerical simulation of marine propeller hydrodynamic performance in uniform inflow with different turbulence models. In *Applied Mechanics and Materials*, 389, 1019-1025.

[15] Sezen, S., Cosgun, T., Yurtseven, A. and Atlar, M, (2021). Numerical investigation of marine propeller underwater radiated noise using acoustic analogy Part 2: The influence of eddy viscosity turbulence models. *Ocean Engineering*, 220.

[16] Wang, L., Wu, T., Gong, J. and Yang, Y., (2021). Numerical simulation of the wake instabilities of a propeller. *Physics of Fluids*, 33(12).

[17] Pawar, S. and Brizzolara, S., (2019). Relevance of transition turbulent model for hydrodynamic characteristics of low Reynolds number propeller. *Applied Ocean Research*, 87, 165-178.

[18] Loureiro, E.V., Oliveira, N.L., Hallak, P.H., de Souza Bastos, F., Rocha, L.M., Delmonte, R.G.P. and de Castro Lemonge, A.C., (2021). Evaluation of low fidelity and CFD methods for the aerodynamic performance of a small propeller. *Aerospace Science and Technology*, 108.

[19] Jiang, Y., Li, Y., Wu, C., Qing, W. and Zhang, G., (2021). Assessment of RANS and DES turbulence models for the underwater vehicle wake flow field and propeller excitation force. *Journal of Marine Science and Technology*, 27, 226-244.

[20] Tu, T.N., (2019). Numerical simulation of propeller open water characteristics using RANSE method. *Alexandria Engineering Journal*, 58(2), 531-537.

[21] Yang, X.I. and Griffin, K.P. (2021) Grid-point and time-step requirements for direct numerical simulation and large-eddy simulation. *Physics of Fluids*, 33(1).

[22] Lew, A.J., Buscaglia, G.C. and Carrica, P.M., (2001). A note on the numerical treatment of the k-epsilon turbulence model. *International Journal of Computational Fluid Dynamics*, 14(3), 201-209.

[23] Balabel, A. and El-Askary, W.A., (2011). On the performance of linear and nonlinear k–ε turbulence models in various jet flow applications. *European Journal of Mechanics-B/Fluids*, 30(3), 325-340.

[24] Shih, T.H., Liou, W.W., Shabbir, A., Yang, Z. and Zhu, J., (1995). A new k-e eddy viscosity model for high reynolds number turbulent flows. *Computers & fluids*, 24(3), 227-238.

[25] Yakhot, V.S., Orszag, S.A., Thangam, S., Gatski, T.B. and Speziale, C., (1992). Development of turbulence models for shear flows by a double expansion technique. *Physics of Fluids A: Fluid Dynamics*, 4(7), 1510-1520.

[26] Morgans, R.C, Dally, B.B, Nathan, G.J, Lanspeary, P.V, Fletcher, D.F, (1999). Application of the reviesed Wilcox (1998) k-w turbulence model to a jet in Co-Flow, *Second International Conference on CFD in Materials and Process Industries*, 479-484.

[27] Adanta, D., Fattah, I.R. and Muhammad, N.M., (2020). Comparison of standard k-epsilon and

sst k-omega turbulence model for breastshot waterwheel simulation. *Journal of Mechanical Science and Engineering*, 7(2), 39-44.

[28] Zhang, C., Bounds, C.P., Foster, L. and Uddin, M., (2019). Turbulence modeling effects on the CFD predictions of flow over a detailed full-scale sedan vehicle. *Fluids*, 4(3).

[29] Menter, F.R. (1994) Two-equation eddy-viscosity turbulence models for engineering applications. *AIAA J*. 32, 1598–1605.

[30] Yang, X.L., Liu, Y. and Yang, L., (2020). A shear stress transport incorporated elliptic blending turbulence model applied to near-wall, separated and impinging jet flows and heat transfer. *Computers & Mathematics with Applications*, 79(12), 3257-3271.

[31] Chiroșcă, A.M. and Rusu, L., (2021). Comparison between model test and three CFD studies for a benchmark container ship. *Journal of Marine Science and Engineering*, 9(1), 62.

[32] Spalart, P. and Allmaras, S., (1992). January. A one-equation turbulence model for aerodynamic flows. *In 30th aerospace sciences meeting and exhibit*, 439.

[33] Lorin, E., Ben Haj Ali, A. and Soulaimani, A., (2006). An accurate positivity preserving scheme for the Spalart-Allmaras turbulence model. Application to aerodynamics. *In 36th AIAA Fluid Dynamics conference and exhibit*, 374.

[34] Kostić, Č., (2015). Review of the Spalart-Allmaras turbulence model and its modifications to three-dimensional supersonic configurations. *Scientific Technical Review*, 65(1), 43-49.

[35] Casseer, D. and Ranasinghe, C., (2019). Assessment of spallart almaras turbulence model for numerical evaluation of ceiling fan performance. *In 2019 Moratuwa Engineering Research Conference*, 577-582.

[36] Paciorri, R., Dieudonne, W., Degrez, G., Charbonnier, J.M., Deconinck, H., Paciorri, R., Dieudonne, W., Degrez, G., Charbonnier, J.M. and Deconinck, H., (1997). Validation of the Spalart-Allmaras turbulence model for application in hypersonic flows. *In 28th Fluid Dynamics Conference*, 202.

[37] Medida, S. and Baeder, J, (2011). Application of the correlation-based gamma-re theta t transition model to the spalart allmaras turbulence model. *In 20th AIAA computational fluid dynamics conference*, 3979.

[38] Stajuda, M., Karczewski, M., Obidowski, D. and Jóźwik, K., (2016). Development of a CFD model for propeller simulation. *Mechanics and Mechanical Engineering*, 20(4), 579-593.

[39] Caradonna, F.X. and Tung, C., (1981). Experimental and analytical studies of a model helicopter rotor in hover. *In European rotorcraft and powered lift aircraft forum*, 8332.